Eur. Phys. J. C 36, 201–213 (2004)
Digital Object Identifier (DOI) 10.1140/epjc/s2004-01894-1

THE EUROPEAN PHYSICAL JOURNAL C

Threshold corrections in bottom and charm quark hadroproduction at next-to-next-to-leading order

N. Kidonakis[1], R. Vogt[2,3]

[1] Cavendish Laboratory, University of Cambridge, Madingley Road, Cambridge CB3 0HE, UK
[2] Nuclear Science Division, Lawrence Berkeley National Laboratory, Berkeley, CA 94720, USA
[3] Physics Department, University of California at Davis, Davis, CA 95616, USA

Received: 26 April 2004 /
Published online: 2 July 2004 –

Abstract. We calculate threshold soft-gluon corrections to total cross sections and transverse momentum distributions for bottom and charm quark production in fixed target experiments, considering both pp and $\pi^- p$ interactions. We investigate the quality of the near-threshold soft-gluon approximation at next-to-leading order (NLO) and calculate next-to-next-to-leading order (NNLO) corrections through next-to-next-to-next-to-leading-logarithmic (NNNLL) accuracy, including some virtual terms. We find that the NNLO threshold corrections reduce the factorization and renormalization scale dependence of the cross sections.

1 Introduction

The latest calculations for heavy quark hadroproduction have included next-to-next-to-leading-order (NNLO) soft-gluon corrections to the double differential cross section [1–5] from threshold resummation techniques [6–8]. These resummations are a consequence of the factorization properties of QCD which separate cross sections into universal non-perturbative parton densities and a perturbatively-calculable partonic cross section. Near threshold there is limited phase space for the emission of real gluons so that soft-gluon corrections dominate the cross section. These Sudakov corrections have the form of logarithmic plus distributions, singular at partonic threshold. Threshold resummation techniques organize these singular distributions to all orders, thus extending the reach of QCD into the near-threshold region.

Calculations of bottom and especially charm production are still not under solid theoretical control. A good understanding of the bottom cross section is important for HERA-B, where b-quark production is near threshold. The charm cross section is of particular interest for heavy ion physics. Although many future heavy ion experiments will be at high collider energies, $\sqrt{S} \geq 130\,\mathrm{GeV}$, some of the current and future experiments, like those at the SPS, are in the near-threshold region. The NA60 experiment will take heavy ion data at $\sqrt{S} = 17.3\,\mathrm{GeV}$ and pA data at $\sqrt{S} = 29.1\,\mathrm{GeV}$. A new facility is being built at the GSI [9] that will measure charm near threshold with $\sqrt{S} = 6.98\,\mathrm{GeV}$.

Because the charm quark mass is a few times Λ_{QCD}, it is generally treated as a heavy quark in perturbative QCD calculations. However, its relative lightness results in a rather strong mass and scale dependence for the total cross section. There is also a rather broad spread in the charm production cross section data at fixed target energies.

In this paper, we increase the accuracy of previous soft-gluon calculations for bottom and charm production. The soft corrections that we calculate take the form of logarithms, $[\ln^l(x_{\mathrm{th}})/x_{\mathrm{th}}]_+$, with $l \leq 2n-1$ for the order α_{s}^n corrections, where x_{th} is a kinematical variable that measures distance from threshold and goes to zero at threshold. NNLO calculations ($n = 2$) for bottom and charm quark production have so far been done through next-to-next-to-leading-logarithmic (NNLL) accuracy, i.e. for the scale-independent terms, including leading logarithms (LL) with $l = 3$, next-to-leading logarithms (NLL) with $l = 2$, and NNLL with $l = 1$ [1–4]. In [2–4], heavy quark cross sections were studied in both single-particle-inclusive (1PI) and pair-invariant-mass (PIM) kinematics. Important differences between the two kinematics choices were found in both the parton-level and hadron-level cross sections, even near threshold. Thus subleading, i.e. beyond NNLL, contributions can still have an impact on the cross section. Their inclusion is clearly needed to bring the calculation under further theoretical control. The subleading terms indeed minimize the kinematics dependence of the top quark production cross section [5].

In [1,2] we studied top and bottom quark production at NNLO-NNLL. In [4] we studied charm quark production at NNLO-NNLL. More recently we extended our calculations for top quark production [5], using the methods and results of [10], to include additional subleading NNLO soft corrections, including next-to-next-to-next-to-leading logarithms (NNNLL), with $n = 2$, $l = 0$, as well as some virtual $\delta(x_{\mathrm{th}})$ corrections. We showed in [5] that the sub-

leading corrections do indeed bring the 1PI and PIM results into agreement near threshold for both the $q\overline{q} \to Q\overline{Q}$ and the $gg \to Q\overline{Q}$ channels while the discrepancies away from threshold are also diminished, especially in the gg channel. Thus the threshold region is brought under better theoretical control. In this paper, we apply these new terms to bottom and charm quark production.

In the following section, we briefly discuss the differences between the 1PI and PIM kinematics choices and then investigate which choice is a better approximation to the full NLO result. We find that 1PI kinematics is a far better choice. Thus we only calculate the cross section in this kinematics in the remainder of the paper.

Section 3 discusses bottom quark production in $\pi^- p$ and pp collisions, particularly at HERA-B. We present the hadronic total cross sections for a range of energies near threshold. We also calculate the transverse momentum distributions for bottom production at HERA-B. In Sect. 4 we study charm production in $\pi^- p$ and pp collisions. Our studies focus on the kinematics of the proposed GSI facility and the CERN SPS proton and ion fixed target programs. We conclude with a summary in Sect. 5.

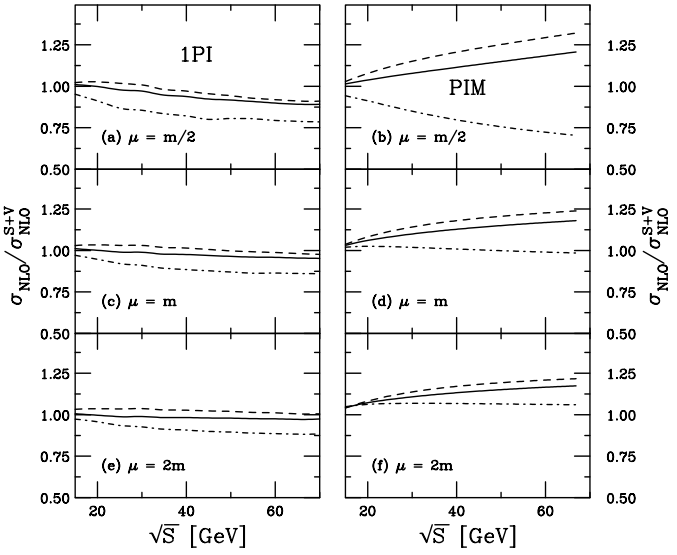

Fig. 1. The ratios of the NLO exact, $\sigma_{\rm NLO}$ over the NLO soft-plus-virtual, $\sigma_{\rm NLO}^{\rm S+V}$, cross sections for bottom quark production with $m = 4.75\,{\rm GeV}$ are shown for the gg (dashed) and $q\overline{q}$ (dot-dashed) channels separately, along with their sum (solid)

2 Singular distributions and kinematics dependence

As we discussed in the introduction, the soft-gluon corrections that we calculate take the form of logarithms, $[\ln^l(x_{\rm th})/x_{\rm th}]_+$, where $x_{\rm th}$ is a kinematical variable that measures the distance from partonic threshold. The exact definition of $x_{\rm th}$ depends on the kinematics we use for the calculation of the cross section.

We study the partonic process $ij \to Q\overline{Q}$ where Q is the produced heavy quark and ij can be either $q\overline{q}$ or gg. A more detailed discussion of the kinematics can be found in [2].

In 1PI kinematics, a single heavy quark is identified so that

$$i(p_a) + j(p_b) \longrightarrow Q(p_1) + X\left[\,\overline{Q}\,\right](p_2) \qquad (2.1)$$

where Q is the identified bottom or charm quark of mass m and $X[\overline{Q}]$ is the remaining final state that contains the heavy antiquark $\overline{Q}$. We define the kinematical invariants $s = (p_a + p_b)^2$, $t_1 = (p_b - p_1)^2 - m^2$, $u_1 = (p_a - p_1)^2 - m^2$ and $s_4 = s + t_1 + u_1$. At threshold, $s_4 \to 0$ and the soft corrections appear as $[\ln^l(s_4/m^2)/s_4]_+$. We note that the virtual corrections multiply $\delta(s_4)$.

In PIM kinematics, we have instead

$$i(p_a) + j(p_b) \longrightarrow Q\overline{Q}(p) + X(k)\,. \qquad (2.2)$$

At partonic threshold, $s = M^2$, M^2 is the pair mass squared, $t_1 = -(M^2/2)(1 - \beta_M \cos\theta)$ and $u_1 = -(M^2/2) \times (1 + \beta_M \cos\theta)$ where $\beta_M = \sqrt{1 - 4m^2/M^2}$ and θ is the scattering angle in the parton–parton center-of-mass frame. The soft corrections appear as $[\ln^l(1-z)/(1-z)]_+$ with $z = M^2/s \to 1$ at threshold. We note that the virtual corrections multiply $\delta(1-z)$.

The effect of the soft-gluon corrections varies depending on the kinematics choice because of uncalculated subleading terms. Thus the quality of the soft-gluon approximation, the extent to which the soft-gluon corrections approximate the full corrections at a given order in $\alpha_{\rm s}$, depends on the kinematics choice even though the full corrections do not depend on the kinematics.

We thus first test the soft-gluon approximation in 1PI and PIM kinematics at NLO. In Fig. 1 we present the ratios of the exact NLO cross sections, $\sigma_{\rm NLO}$, to the approximate soft-plus virtual NLO cross section, $\sigma_{\rm NLO}^{\rm S+V}$, (the Born result plus the $\mathcal{O}(\alpha_{\rm s}^3)$ soft and virtual corrections) for bottom quark production in pp collisions over a range of $\sqrt{S}$ near bottom production threshold. In our calculations we use the MRST2002 NNLO [11] parton densities. We show the ratios in both 1PI and PIM kinematics for each of the two partonic channels separately as well as for their sum for three scale choices: $\mu = m/2, m$, and $2m$. Note that the factorization and renormalization scales are set equal and are both denoted by μ.

It is clear from Fig. 1 that the soft-plus-virtual result is a much better approximation to the exact NLO total cross section in 1PI kinematics than in PIM kinematics over the entire range of energies and scales shown. The same conclusion is reached for charm production, shown in Fig. 2 for pp collisions with $\mu = m$ and $2m$. Since the 1PI kinematics choice is a better approximation to the exact NLO cross section, here we choose to work in this kinematics only.

One-particle inclusive kinematics is a better approximation to the total $b\overline{b}$ and $c\overline{c}$ production cross sections because the gg channel is dominant. For $\mu \geq m$, PIM kinematics gives a better approximation to the NLO $q\overline{q}$ cross section, not unexpected due to the simple color structure of this s-channel process. However, with its more complex

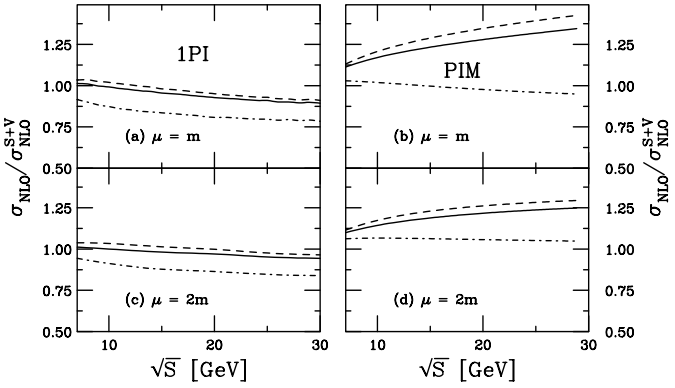

Fig. 2. The ratios of the NLO exact, $\sigma_{\rm NLO}$ over the NLO soft-plus-virtual, $\sigma^{\rm S+V}_{\rm NLO}$, cross sections for charm quark production with $m = 1.5\,{\rm GeV}$ are shown for the gg (dashed) and $q\overline{q}$ (dot-dashed) channels separately, along with their sum (solid)

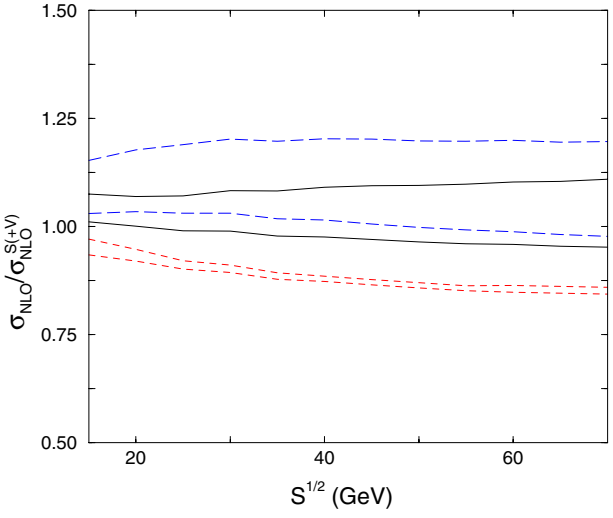

Fig. 3. The ratio of $\sigma_{\rm NLO}/\sigma^{\rm S}_{\rm NLO}$, with the soft-gluon terms alone, and $\sigma_{\rm NLO}/\sigma^{\rm S+V}_{\rm NLO}$, including the virtual terms, are shown for bottom quark production at $\mu = m = 4.75\,{\rm GeV}$. We show the results for the gg channel (long-dashed) with (lower) and without the virtual terms (upper); the $q\overline{q}$ channel (dashed) with (upper) and without the virtual terms (lower); and their sum (solid) with (lower) and without the virtual terms (upper)

color structure, the gg channel is more amenable to the 1PI kinematics choice. We also found that, when the gg channel dominates production, the 1PI scale dependence remains small while the PIM kinematics choice has a large scale dependence, larger than the exact NLO [5].

Finally, we investigate the validity of the threshold approximation if only the soft terms are included and the virtual ones are not. Figure 3 compares the ratios, $\sigma_{\rm NLO}/\sigma^{\rm S}_{\rm NLO}$, with the soft-gluon terms alone, to $\sigma_{\rm NLO}/\sigma^{\rm S+V}_{\rm NLO}$ for bottom quark production in 1PI kinematics with $\mu = m = 4.75\,{\rm GeV}$. We see that even though the ratios with the NLO soft-gluon approximation alone are somewhat farther from one, they are still a rather good estimate of the exact NLO result.

In the following sections we present cross sections for bottom and charm quark production. The LO and NLO results are exact. The NNLO results are approximate and include soft-gluon contributions only. At NNLO we give results both for NNLL accuracy, i.e. for the scale-independent terms, including all $\ln^3(s_4/m^2)/s_4$, $\ln^2(s_4/m^2)/s_4$, and $\ln(s_4/m^2)/s_4$ terms, and for NNNLL+ζ accuracy, which includes, in addition to the NNLL terms, all $1/s_4$ terms (NNNLL) as well as some ζ terms in the virtual corrections. For full details, see [5]. We note that the NNLO-NNNLL+ζ result includes all NNLO soft and virtual terms proportional to the factorization and renormalization scales, while the NNLO-NNLL calculation includes in the virtual contribution only scale-dependent terms proportional to the squares of scale-dependent logarithms.

3 Bottom quark production

The main difficulty in comparing the calculated $Q\overline{Q}$ cross sections to data lies in the fact that charm and bottom quarks hadronize before decaying. Top quark production is much cleaner in this respect since the top quark decays before it can hadronize and the measured cross sections can be compared directly to theory. No attempt has been made to correct B meson measurements to b quark cross sections here.

3.1 b-quark production in $\pi^- p$ interactions

There is not much data on bottom quark hadroproduction at fixed target energies. Some of the earliest data were from $\pi^- A$ interactions where A is a nucleus. A linear A dependence was typically assumed. The data [12–16] are shown in Fig. 4 along with our calculations. The NA10 point at $\sqrt{S} = 19.7\,{\rm GeV}$ is a compilation of data taken at 140, 194 and 286 GeV on tungsten targets measuring trimuons [12]. They quote a $B\overline{B}$ cross section essentially independent of energy. The x_F distribution of the B mesons was assumed to be uniform around $x_F = 0$ with a cross section proportional to $(1-|x_F|)^3$. Assumptions regarding the shape of the distribution and the decay branching ratios almost certainly overestimate the cross section. The other data is analyzed using the B decay to J/ψ. The WA78 data, taken with 320 GeV π^- beams on a uranium target, used several hypotheses regarding production models and B^0–$\overline{B}^0$ mixing angles. The data point shown assumes the largest $\langle x_F\rangle$ and the maximal mixing. It is the smallest cross section reported in [13]. The WA92 data were taken at 350 GeV on a copper target [14]. The E653 data were taken with a 600 GeV beam on emulsion [15] while the E672 data at 515 GeV was taken on a beryllium target [16]. Only this latter point used a NLO calculation to extrapolate from $x_F > 0$, where the data were taken, to all x_F. All these data rely on relatively few events and some of the assumptions should be taken with a grain of salt.

Figure 4 presents the energy dependence of the production cross sections as functions of both bottom quark mass and scale. We use the GRV98 HO proton parton densities [17] with the GRS pion densities [18]. The GRS pion

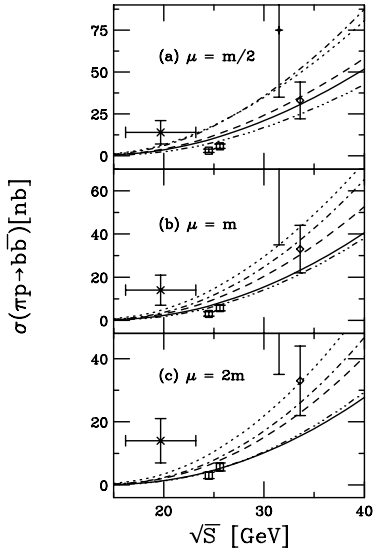

Fig. 4. The energy dependence of $b\bar{b}$ production in $\pi^- p$ collisions with **a** $\mu = m/2$, **b** $\mu = m$ and **c** $\mu = 2m$, calculated with the GRV98 HO proton densities and the GRS pion densities. We show the NLO (solid) and 1PI NNLO-NNLL (dot-dashed) results at $m = 4.75\,\text{GeV}$. The 1PI NNLO-NNNLL+ζ results are shown for $m = 4.75$ (dashed), 4.5 (dotted) and 5 (dot-dot-dot-dashed) GeV

densities, produced in 1999, are the most recent set of pion densities and are compatible with the GRV98 densities. We do not use other proton densities because there are no recent equivalent pion sets.

Since the bottom quark mass is relatively large, we vary the scale between $m/2$ and $2m$ in Fig. 4. For our central value of the bottom quark mass, $m = 4.75\,\text{GeV}$, we present the exact NLO cross section (solid curve), the 1PI NNLO-NNLL cross section (dot-dashed) and the 1PI NNLO-NNNLL+ζ cross section (dashed). We also show the 1PI NNLO-NNNLL+ζ cross sections for $m = 4.5\,\text{GeV}$ (dotted) and 5 GeV (dot-dot-dot-dashed). Because we focus on the NNLO-NNNLL+ζ results here, we do not present the NLO and NNLO-NNLL cross sections for the lower and upper mass values in Fig. 4.

It is difficult to quantitatively compare the calculations to the data because the data are not really compatible with each other. Therefore our discussion is only on a qualitative level. Note that, at $m = 4.75\,\text{GeV}$, the 1PI NNLO-NNNLL+ζ result is intermediate to the exact NLO and the 1PI NNLO-NNLL cross sections. The subleading terms reduce the overall NNLO corrections, resulting in a value near the average of the 1PI and PIM NNLO-NNLL cross sections. The $m = 4.5\,\text{GeV}$ 1PI NNLO-NNNLL+ζ cross section is typically equivalent to ($\mu = m/2$) or larger than ($\mu \geq m$) the $m = 4.75\,\text{GeV}$ 1PI NNLO-NNLL cross section while the 5 GeV result is similar to the exact NLO cross section for $m = 4.75\,\text{GeV}$. Changing the bottom quark mass between 4.5 and 5 GeV changes the 1PI NNLO-NNNLL+ζ cross sections by a factor of two.

Near threshold, $\pi^- p \to b\bar{b}$ production is dominated by the $q\bar{q}$ channel, due to the valence quark–valence antiquark contribution at large momentum fractions [19]. The $q\bar{q}$ channel gives the largest contribution to the $b\bar{b}$ cross section for $\sqrt{S} \leq 40\,\text{GeV}$, the range shown in Fig. 4.

We now discuss the convergence properties of the subleading terms. Various definitions of the "first-order K factor", $K^{(1)} = \sigma_{\text{NLO}}/\sigma_{\text{LO}}$, were discussed in [20]. In [3,4], we compared two of these definitions, $K_0^{(1)}$, where σ_{LO} was calculated with NLO parton densities and a two-loop evaluation of α_s, and $K_2^{(1)}$, where σ_{LO} was calculated with LO parton densities and a one-loop evaluation of α_s. In both cases, the Born and $\mathcal{O}(\alpha_s^3)$ contributions to σ_{NLO} were calculated with NLO parton densities and two-loop evaluations of α_s. The first definition, $K_0^{(1)}$, indicates the convergence of terms in a fixed-order calculation while the second, $K_2^{(1)}$, indicates the convergence of the hadronic calculation towards a result. Since a NNLO set of parton densities has recently become available, in this paper, we will use both NLO and NNLO parton densities to calculate $K_0^{(1)}$. Thus when the NNLO densities are used, σ_{LO} in $K_0^{(1)}$ is calculated with the NNLO parton densities and a three-loop evaluation of α_s. The definition of $K_0^{(1)}$ then indicates the convergence of terms in a fixed-order calculation for a given set of parton densities. We compare $K_0^{(1)}$ to the 1PI NNLO K factors, $K^{(2)} = \sigma_{\text{NNLO-NNLL}}/\sigma_{\text{NLO}}$ and $K_{\text{sub}}^{(2)} = \sigma_{\text{NNLO-NNNLL+}\zeta}/\sigma_{\text{NLO}}$; the latter includes the new subleading terms. In each case, the NNLO K factors are either calculated with NLO or NNLO parton densities and a two-loop or three-loop evaluation of α_s at each order. If $K^{(2)}$ or $K_{\text{sub}}^{(2)}$ is less than $K_0^{(1)}$, then convergence of the perturbative expansion is indicated.

The results for $\pi^- p \to b\bar{b}$ production are shown in Fig. 5 as a function of energy. We present the K factors for $m = 4.75$ GeV only since the results are very similar for the other masses. All the K factors are calculated with the GRV98 HO proton parton densities and the GRS pion parton densities.

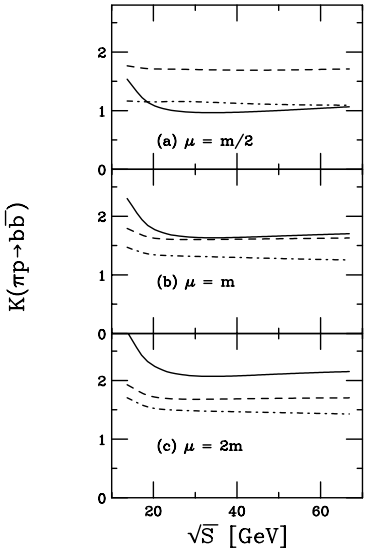

Fig. 5. The K factors for $b\bar{b}$ production in $\pi^- p$ collisions with $m = 4.75\,\text{GeV}$. We present $K_0^{(1)}$ (solid), $K^{(2)}$ (dashed) and $K_{\text{sub}}^{(2)}$ (dot-dashed) results for **a** $\mu = m/2$, **b** $\mu = m$ and **c** $\mu = 2m$

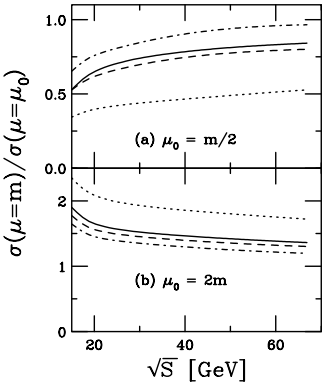

Fig. 6. The scale dependence of $b\bar{b}$ production in $\pi^- p$ collisions with $m = 4.75\,\text{GeV}$. We give the ratios $\sigma(\mu = m)/\sigma(\mu = \mu_0)$ for the LO (dotted), NLO (solid), 1PI NNLO-NNLL (dashed) and 1PI NNLO-NNNLL+ζ (dot-dashed) cross sections. The results with $\mu_0 = m/2$ are given in **a** while the results with $\mu_0 = 2m$ are given in **b**

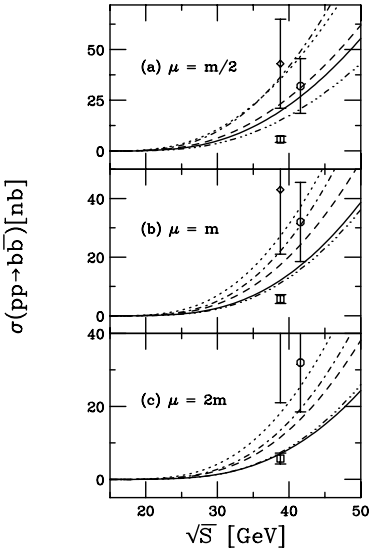

Fig. 7. The energy dependence of $b\bar{b}$ production in pp collisions with **a** $\mu = m/2$, **b** $\mu = m$ and **c** $\mu = 2m$, calculated with the GRV98 HO proton densities. We show the NLO (solid) and 1PI NNLO-NNLL (dot-dashed) results at $m = 4.75\,\text{GeV}$. The 1PI NNLO-NNNLL+ζ results are shown for $m = 4.75$ (dashed), 4.5 (dotted) and 5 (dot-dot-dot-dashed) GeV

Note that $K_0^{(1)}$ has the strongest energy dependence with a minimum around $\sqrt{S} = 20\,\text{GeV}$, higher at lower $\sqrt{S}$ and slowly increasing with $\sqrt{S}$ above 20 GeV. We find $K_0^{(1)} \approx 1$ for $\mu = m/2$, increasing to ≈ 2.1 at $\mu = 2m$. The 1PI NNLO-NNLL K factors, $K^{(2)}$, the dashed curves, are flatter but $K^{(2)}$ is larger than $K_0^{(1)}$ when $\mu = m/2$. However, $K^{(2)}$ is nearly independent of scale and energy. Including the subleading terms increases the scale dependence of $K_{\text{sub}}^{(2)}$ slightly but $K_{\text{sub}}^{(2)} < K^{(2)}$ for all energies, $K_{\text{sub}}^{(2)} \approx 1.1$ for $\mu = m/2$ and ≈ 1.4 for $\mu = 2m$. Note that $K^{(2)}$ and $K_{\text{sub}}^{(2)}$ are both nearly independent of $\sqrt{S}$ except for $\sqrt{S} < 20\,\text{GeV}$. The small $q\bar{q}$ NNLO corrections reduce the increase of the K factor at low $\sqrt{S}$.

Another measure of convergence is the scale dependence. Going to higher orders should make the result increasingly independent of scale. We found this to be true for $t\bar{t}$ production at the Tevatron [5]. Here we show the scale dependence as a function of energy for the ratio $\sigma(\mu = m)/\sigma(\mu = \mu_0)$ where $\mu_0 = m/2$ in the upper plot and $2m$ in the lower. Since $\sigma(\mu = m) < \sigma(\mu = m/2)$, the upper ratio is less than unity. Thus an increasing independence of scale would make the ratio approach unity from below as the cross section is calculated to higher orders. The scale dependence is indeed decreasing for the 1PI NNLO-NNNLL+ζ cross section over all energies. This is a significant improvement over the NNLO-NNLL result alone, further from unity than the NLO ratio. Improvement is also seen for $\mu_0 = 2m$ where the ratio should approach unity from above.

3.2 b-quark production in pp interactions

We now turn to pp production of bottom quarks. So far, three experiments have reported the $b\bar{b}$ total cross section in proton-induced fixed target interactions [22–24], all at similar energies. The cross sections are all based on relatively small event samples. There are two measurements at 800 GeV, the E789 result, using a gold target [22], and the E771 result, using a silicon target [23]. There is a rather large difference between the two reported cross sections. The E771 measurement is in agreement with the HERA-B measurement at 920 GeV, taken on carbon and titanium targets [24]. All three experiments use the J/ψ decay channel.

The three data points are compared to our calculations with the GRV98 HO proton parton densities in Fig. 7 and with the MRST2002 NNLO parton densities in Fig. 8. The results are again shown for the exact NLO, 1PI NNLO-NNLL and 1PI NNLO-NNNLL+ζ cross sections at $m = 4.75\,\text{GeV}$ as well as the 1PI NNLO-NNNLL+ζ cross sections at $m = 4.5$ and 5 GeV.

The gg channel dominates $b\bar{b}$ production in pp collisions over the entire energy region shown. Note that the $pp \to b\bar{b}$ cross section is considerably smaller than the $\pi^- p \to b\bar{b}$ cross section in the near-threshold region. The $\pi^- p$ cross section is larger because of the high valence quark–valence antiquark luminosity, absent in pp collisions. At higher energies, far above threshold, the cross sections in both processes become more similar. Due to the difference in the pion and proton gluon distributions, however, they do not become equal.

The trends in the calculated cross sections are similar to those of Fig. 4. Typically, the 1PI NNLO results with the MRST2002 NNLO parton densities are somewhat larger than those with the GRV98 HO parton densities although the exact NLO results are quite similar. The difference is due to the somewhat larger value of Λ_4 for the MRST2002 NNLO densities. The HERA-B collaboration [24] reported that with $m = 4.75\,\text{GeV}$, $\mu = m$ and the CTEQ5M densities [21], the average of the 1PI and PIM NNLO-NNLL cross sections in [2] was in good agreement with their data. Since

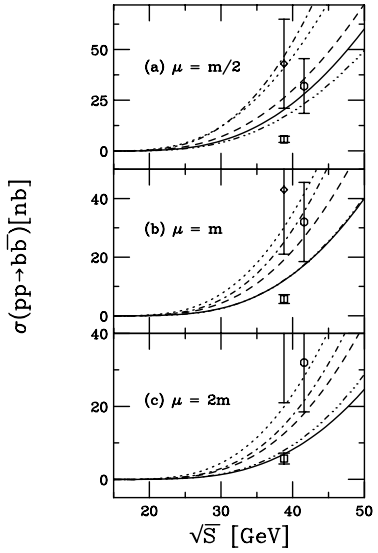

Fig. 8. The energy dependence of $b\bar{b}$ production in pp collisions with **a** $\mu = m/2$, **b** $\mu = m$ and **c** $\mu = 2m$, calculated with the MRST2002 NNLO proton densities. We show the NLO (solid) and 1PI NNLO-NNLL (dot-dashed) results at $m = 4.75\,\mathrm{GeV}$. The 1PI NNLO-NNNLL+ζ results are shown for $m = 4.75$ (dashed), 4.5 (dotted) and 5 (dot-dot-dot-dashed) GeV

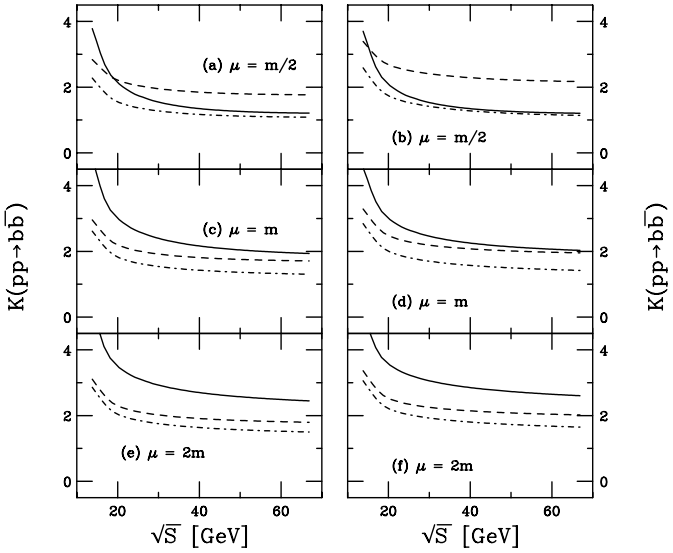

Fig. 9. The K factors for $b\bar{b}$ production in pp collisions with $m = 4.75\,\mathrm{GeV}$. We present $K_0^{(1)}$ (solid), $K^{(2)}$ (dashed) and $K_{\mathrm{sub}}^{(2)}$ (dot-dashed) results for **a** and **b**, $\mu = m/2$, **c** and **d**, $\mu = m$ and, **e** and **f**, $\mu = 2m$. Results with the GRV98 HO proton densities are shown on the left-hand side while results with the MRST2002 NNLO proton densities are shown on the right-hand side

Λ_4 for the CTEQ5M densities is larger than the corresponding values for either the GRV98 or MRST2002 densities, the NNLO contribution is larger for the CTEQ5M densities. The 1PI NNLO-NNNLL+ζ result, similar to the 1PI and PIM average, although slightly lower than the mean reported HERA-B cross section in Figs. 7 and 8 for the same values of m and μ, is still in good agreement.

The NNLO-NNNLL+ζ $b\bar{b}$ cross section at $\sqrt{S} = 41.6\,\mathrm{GeV}$ with the MRST2002 NNLO parton densities is

$$\sigma^{\mathrm{MRST2002NNLO}}_{\mathrm{NNLO-NNNLL+}\zeta} = 28 \pm {}^{+15}_{-10}\ \mathrm{nb}\ . \tag{3.1}$$

The central value represents the result for $m = \mu = 4.75\,\mathrm{GeV}$, the first uncertainty is due to the scale variation and the second is due to the variation in m. The corresponding cross section for the GRV98 densities is somewhat smaller than the MRST result,

$$\sigma^{\mathrm{GRV98}}_{\mathrm{NNLO-NNNLL+}\zeta} = 25^{+7+13}_{-8\ -9}\ \mathrm{nb}\ . \tag{3.2}$$

The uncertainties are also reduced for this density due to the lower value of Λ_4 associated with this set. The NLO cross sections are, on the other hand, essentially identical for the two sets,

$$\sigma_{\mathrm{NLO}} = 17^{+12+10}_{-7\ -6}\ \mathrm{nb}\ . \tag{3.3}$$

The K factors are shown for both sets of parton densities in Fig. 9. Recall that when the MRST2002 NNLO densities are used, all K factors are computed with these densities, as are the cross sections at each order shown in Fig. 8. All the K factors computed with both densities tend to be larger for pp than $\pi^- p$ collisions, especially at lower $\sqrt{S}$. They are also stronger functions of $\sqrt{S}$ than those shown in Fig. 5. The value of $K_0^{(1)}$ is larger than $K^{(2)}$ except for $\mu = m/2$. Note that $K_{\mathrm{sub}}^{(2)}$ is less than $K_0^{(1)}$ and $K^{(2)}$ for all scales. We see that $K^{(2)}$ is nearly scale independent but has a value of ≈ 2, still rather large. Including subleading terms gives $K_{\mathrm{sub}}^{(2)} \approx 1$ for $\sqrt{S} \geq 20\,\mathrm{GeV}$ and $\mu = m/2$, increasing to ≈ 1.6 for $\mu = 2m$. The values of K are nearly independent of the parton densities and bottom quark mass in all cases.

Figure 10 shows the scale dependence of $b\bar{b}$ production in pp collisions for both sets of parton densities. We again find a reduction of the scale dependence for the 1PI NNLO-NNNLL+ζ results over all energies. Improvement in the approach of the ratio $\sigma(\mu = m)/\sigma(\mu = \mu_0)$ toward unity is seen relative to the 1PI NNLO-NNLL cross section ratio when $\mu_0 = m/2$. The latter ratio is smaller than the NLO ratio, indicating stronger scale dependence for the 1PI NNLO-NNLL cross section than that of the exact NLO result. Clear improvement is also seen for $\mu_0 = 2m$.

In Fig. 11, we plot the scale dependence for $0.3 < \mu/m < 10$ with $\sqrt{S} = 41.6\,\mathrm{GeV}$ and $m = 4.75\,\mathrm{GeV}$. We show results for the Born, NLO, and NNLO-NNNLL+ζ cross sections. The scale dependence decreases with increasing order of the cross section. There is no plateau in the Born cross section while the exact NLO and the NNLO-NNNLL+ζ cross sections do show a peak in μ/m. The plateau at $\mu/m \approx 0.4$ is broader for the NNLO-NNNLL+ζ cross section and the overall scale dependence is reduced relative to the exact NLO cross section.

Figure 12 shows the b-quark transverse momentum distribution at HERA-B with $\sqrt{S} = 41.6\,\mathrm{GeV}$ and $m =$

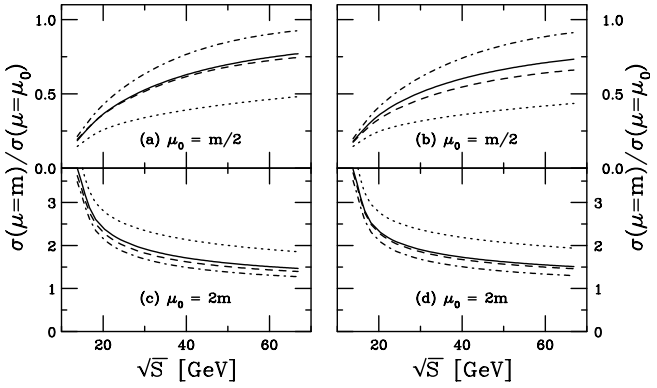

Fig. 10. The scale dependence of $b\bar{b}$ production in pp collisions with $m = 4.75\,\mathrm{GeV}$. We give the ratios $\sigma(\mu = m)/\sigma(\mu = \mu_0)$ for the LO (dotted), NLO (solid), 1PI NNLO-NNLL (dashed) and 1PI NNLO-NNNLL+ζ (dot-dashed) cross sections. The results with $\mu_0 = m/2$ are given in **a** and **b** while the results with $\mu_0 = 2m$ are given in **c** and **d**. Results with the GRV98 HO proton distributions are shown on the left-hand side while results with the MRST2002 NNLO proton distributions are shown on the right-hand side

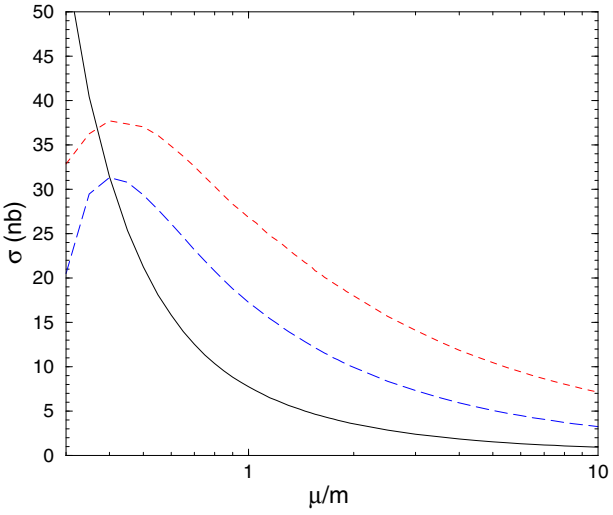

Fig. 11. The bottom quark cross section as a function of μ/m in pp collisions with $\sqrt{S} = 41.6\,\mathrm{GeV}$, $m = 4.75\,\mathrm{GeV}$ and the MRST2002 NNLO densities. The Born (solid), NLO (long-dashed), and NNLO-NNNLL+ζ (dashed) results are shown

4.75 GeV. The Born, NLO, and NNLO-NNNLL+ζ results are shown on the left-hand side. On the right-hand side we plot $K_0^{(1)}$ and $K_{\mathrm{sub}}^{(2)}$. We provide results with two different scales, $\mu = m$ and $\mu = m_{\mathrm{T}} \equiv \sqrt{p_{\mathrm{T}}^2 + m^2}$. There is some difference in the results with the two scales at larger values of p_{T}. The distributions with the fixed scale, $\mu = m$, are somewhat higher than those with $\mu = m_{\mathrm{T}}$. Increasing p_{T} and thus m_{T} decreases α_{s}, reducing $\mathrm{d}\sigma/\mathrm{d}p_{\mathrm{T}}$ at higher p_{T} relative to the fixed scale choice. Although evolution increases the parton densities at low x, at the higher momentum fractions relevant here, evolution decreases the densities at higher scales. Both the running of α_{s} with scale and the evolution of the parton densities work to decrease the cross sections with the running scale relative to the fixed scale at higher p_{T}. With both choices, we see an enhancement of the bottom quark transverse momentum distribution similar to that of the total cross sections when the threshold corrections are added. The shapes of the distributions, however, are very similar [1, 25].

The K factors are, on average, similar to those shown in Fig. 9 at the same energy. When $\mu = m$, both K factors tend to decrease with p_{T} over the range shown. As p_{T} increases, the parton momentum fractions, x, probed also increases reducing both the available phase space and the gg contribution to the cross section. These two effects work together to reduce the K factors at larger p_{T} [26]. When $\mu = m_{\mathrm{T}}$, both K factors are essentially constant, as also seen in [26].

4 Charm quark production

We now turn to charm quark production. There is much more data on charm than bottom production. However, the early data are all rather low statistics and have not been updated to include the latest branching ratios. In our previous report on charm production to NNLO-NNLL [4], we incorporated all the data as published, making assumptions only on how to extrapolate from the measured D meson cross sections to the charm quark cross sections. In this paper we choose only to compare our results to the $\pi^- p$ and pp data tabulated in [27, 28]. These data are the most recent and incorporate the newest measurements of branching ratios. The $\pi^- p$ data in the threshold region, $\sqrt{S} \leq 30\,\mathrm{GeV}$, in order of increasing $\sqrt{S}$ are found in [29–33] while the pp data in the same energy region are given in [29, 30, 34].

How the $c\bar{c}$ pairs hadronize is a particularly important question for energies near threshold where some channels may be energetically disfavored. We follow [27] and assume that $\sigma(D_s)/\sigma(D^0 + D^+) \simeq 0.2$ and $\sigma(\Lambda_c)/\sigma(D^0 + D^+) \simeq 0.3$, independent of energy, so that the total $c\bar{c}$ cross section is obtained from $\approx 1.5\,\sigma(D\overline{D})$. This assumption could have a strong energy dependence near threshold. Thus as many charm hadrons (mesons and baryons) as possible should be measured to better understand fragmentation and hadronization. Finally, some of the data are taken on nuclear targets and then extrapolated to $\pi^- p$ and pp assuming a linear A dependence [35, 36].

Recent comparisons of the full $pp \to c\bar{c}$ data set with exact NLO cross sections were made to determine the best mass and scale choices for extrapolation to higher energies [37]. Rough agreement with the data up to the top ISR energy, $\sqrt{S} = 63\,\mathrm{GeV}$, was found for $m = 1.2\,\mathrm{GeV}$ and $\mu = 2m$ for the MRST densities and $m = 1.3\,\mathrm{GeV}$ with $\mu = m$ for the GRV98 densities [37]. These values of m are rather small compared to the typical value of 1.5 GeV. Thus, as in our previous paper [4], we calculate the NLO, 1PI NNLO-NNLL and, in addition here, the 1PI NNLO-NNNLL+ζ cross sections using $m = 1.2$, 1.5 and 1.8 GeV as well as $\mu = m$ and $2m$. We can then test whether the NNLO+NNNLL+ζ cross sections might favor a higher charm quark mass. Our charm calculations also employ the GRV98 HO and MRST2002 NNLO proton parton densities.

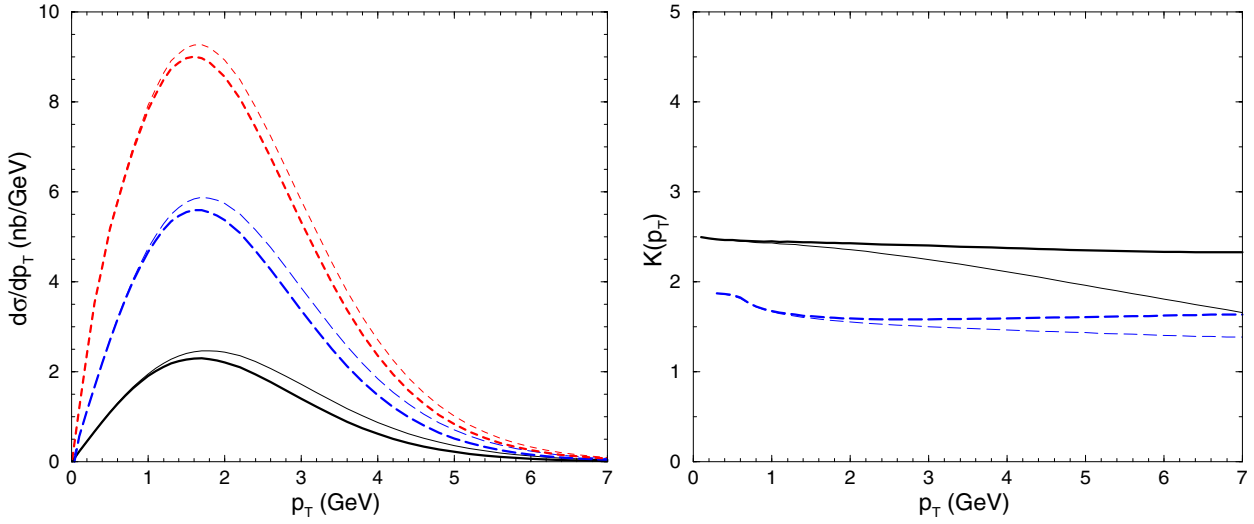

Fig. 12. The bottom quark transverse momentum distributions at $\sqrt{S} = 41.6\,\text{GeV}$, $m = 4.75\,\text{GeV}$ and the MRST2002 NNLO parton densities. On the left-hand side we show the Born (solid), NLO (long-dashed), and NNLO-NNNLL+ζ (dashed) results while on the right-hand side we present $K_0^{(1)}$ (solid) and $K_{\text{sub}}^{(2)}$ (dashed). The bold lines are calculated with $\mu = m_{\text{T}}$ while the thin lines are with $\mu = m$

4.1 Charm production in $\pi^- p$ interactions

We first discuss the results from $\pi^- p$ interactions. These data are typically reported as the forward cross sections, $x_F > 0$. The cross section is extrapolated to all x_F assuming that $\sigma(\text{all } x_F) = 1.6\sigma(x_F > 0)$, calculated to NLO. The difference is not a factor of two as in pp production since the forward x_F distribution is harder than the backward distribution due to the harder large x behavior of the pion gluon distribution.

The reaction $\pi^- p \to c\bar{c}$ is dominated by the gg channel for $\sqrt{S} \geq 15\,\text{GeV}$ [19]. The gg and $q\bar{q}$ channels are only similar in magnitude very close to threshold. The comparison of the data with the exact NLO, 1PI NNLO-NNLL and 1PI NNLO-NNNLL+ζ cross sections, calculated with the GRV98 HO proton parton densities and the GRS pion parton densities, is shown in Fig. 13. The exact NLO and the 1PI NNLO-NNLL results were previously shown in [4]. The new 1PI NNLO-NNNLL+ζ results, indicated by the dot-dashed curves, are similar to the average of the NNLO-NNLL 1PI and PIM cross sections of [4]. At the higher end of the $\sqrt{S}$ range studied, the new results with the subleading logs are higher than this average because the PIM NNLO-NNLL gg contribution is large and negative above threshold. Eventually this contribution becomes larger than the exact NLO cross section, resulting in a negative PIM NNLO-NNLL total cross section and a decreased 1PI and PIM average NNLO-NNLL cross section, particularly for the lower values of m. Inclusion of the subleading logs mitigates this behavior [5] albeit not enough to make the PIM calculation reliable for gluon dominated processes.

There is relatively good agreement between the exact NLO calculations and the data for $m = 1.2\,\text{GeV}$ and $\mu = 2m$, Fig. 13b. We can see, however, that the data are also relatively compatible with the 1PI NNLO cross sections, both the NNLO-NNLL and NNLO-NNNLL+ζ calculations, when $m = \mu = 1.5\,\text{GeV}$. This result suggests

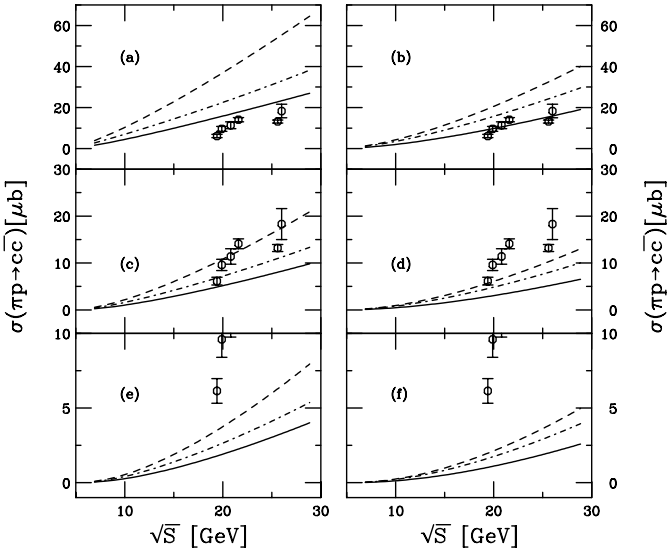

Fig. 13. The energy dependence of $c\bar{c}$ production in $\pi^- p$ collisions with, **a** and **b**, $m = 1.2$, **c** and **d**, $m = 1.5$, and, **e** and **f**, $m = 1.8\,\text{GeV}$, calculated with the GRV98 HO proton densities and the GRS pion densities. We show the NLO (solid), 1PI NNLO-NNLL (dashed) and 1PI NNLO-NNNLL+ζ (dot-dashed) results. On the left-hand side, $\mu = m$ while on the right-hand side, $\mu = 2m$

that a full NNLO calculation would be more compatible with a larger charm quark mass.

The $\pi^- p$ charm production K factors are shown in Fig. 14. As expected, the K factors are all larger for charm than bottom production due to the dominance of the gg channel over all $\sqrt{S}$ as well as the larger value of α_{s}. There is a significant decrease in the K factor when the subleading terms are included: $K_{\text{sub}}^{(2)} \approx 1.5$ whereas $K^{(2)} \approx 2$. All the K factors decrease slightly with increasing m. The mass effect is smaller on $K_0^{(1)}$ than on $K^{(2)}$, the 1PI NNLO-

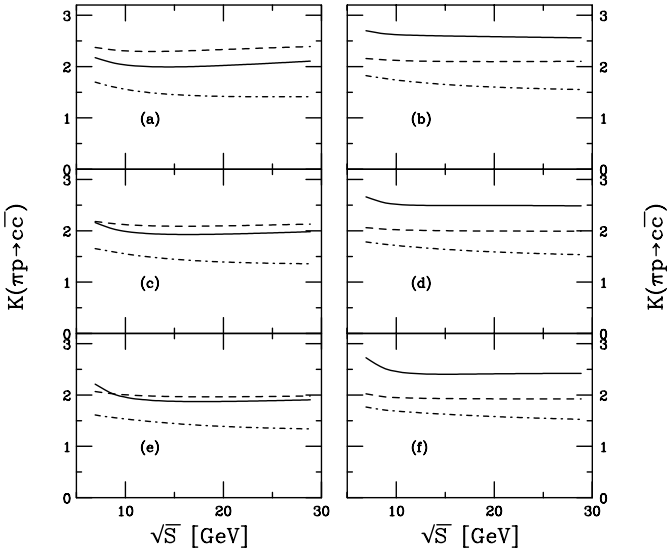

Fig. 14. The K factors for $c\bar{c}$ production in $\pi^- p$ collisions with, **a** and **b**, $m = 1.2$, **c** and **d**, $m = 1.5$, and, **e** and **f**, $m = 1.8\,\mathrm{GeV}$. We present $K_0^{(1)}$ (solid), $K^{(2)}$ (dashed) and $K_{\mathrm{sub}}^{(2)}$ (dot-dashed) for $\mu = m$ (left-hand side) and $\mu = 2m$ (right-hand side)

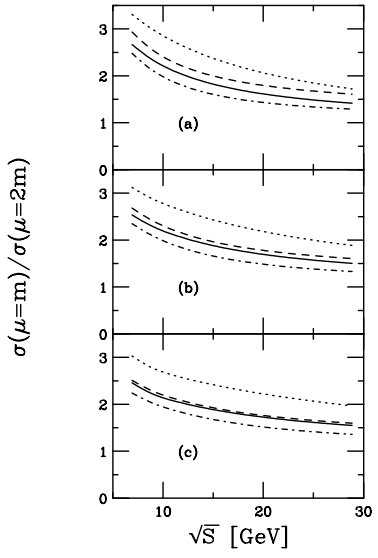

Fig. 15. The scale dependence of $c\bar{c}$ production in $\pi^- p$ collisions with **a** $m = 1.2$, **b** $m = 1.5$, and **c** $m = 1.8\,\mathrm{GeV}$. We give the ratios $\sigma(\mu = m)/\sigma(\mu = 2m)$ for the LO (dotted), NLO (solid), 1PI NNLO-NNLL (dashed) and 1PI NNLO-NNNLL+ζ (dot-dashed) cross sections

NNLL K factor. Indeed the $K^{(2)}$ mass dependence is larger than either that of $K_0^{(1)}$ or $K_{\mathrm{sub}}^{(2)}$. The exact NLO K factor, $K_0^{(1)}$, shows the strongest scale dependence, increasing from ≈ 2 for $\mu = m$ to ≈ 2.5 when $\mu = 2m$, as also seen for $b\bar{b}$ production. Note also that while all the K factors are relatively energy independent, $K_0^{(1)}$ exhibits the largest $\sqrt{S}$ dependence.

Figure 15 demonstrates the scale dependence of charm production in $\pi^- p$ interactions. Since $\mu = m/2$ is less than the initial scale of most sets of parton densities, this value of μ is essentially meaningless for charm production. Therefore, we plot the ratio $\sigma(\mu = m)/\sigma(\mu = 2m)$ as a function of $\sqrt{S}$ for all three values of m. The scale dependence only weakly depends on charm mass although the dependence is slightly stronger at low $\sqrt{S}$. The 1PI NNLO-NNNLL+ζ ratio shows significant improvement over both the NLO and the 1PI NNLO-NNLL results.

4.2 Charm production in pp interactions

We now consider $pp \to c\bar{c}$ interactions. In Figs. 16 and 17, we compare the exact NLO, 1PI NNLO-NNLL and 1PI NNLO-NNNLL+ζ cross sections calculated with the GRV98 HO and MRST2002 NNLO proton parton densities respectively. There is a larger difference between the results with the two parton densities than seen for $b\bar{b}$ production. Since $\Lambda_3 > \Lambda_4$ the overall NNLO corrections are thus larger for charm than bottom as well, as evident from the larger charm K factors. At NLO, the best agreement is again with $m = 1.2\,\mathrm{GeV}$ and $\mu = 2m$, seen in Figs. 16 and 17b. The new result in Fig. 16 is the subleading NNLO-NNNLL+ζ cross section, the other calculations, also shown in [4], are repeated for comparison purposes. The results in Fig. 17 are all new.

The MRST2002 NNLO parton densities generally give larger cross sections, even for the exact NLO result since the value of Λ_3 is larger than that of the GRV98 HO set. Also due the larger Λ_3, the NNLO corrections are significantly larger, as seen in Fig. 17. A similar effect was seen in the comparison of the GRV98 HO and CTEQ5M results in [4].

In both Figs. 16 and 17, the exact NLO cross sections calculated with $m = 1.2\,\mathrm{GeV}$ and $\mu = 2m$ are relatively compatible with the data. Note that in Fig. 16b, the 1PI NNLO-NNNLL+ζ result is in somewhat better agreement

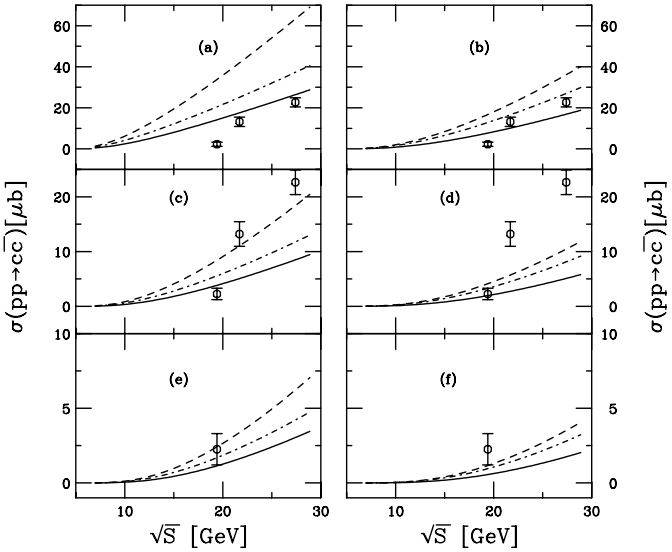

Fig. 16. The energy dependence of $c\bar{c}$ production in pp collisions with, **a** and **b**, $m = 1.2$, **c** and **d**, $m = 1.5$, and, **e** and **f**, $m = 1.8\,\mathrm{GeV}$, calculated with the GRV98 HO proton densities. We show the NLO (solid), 1PI NNLO-NNLL (dashed) and 1PI NNLO-NNNLL+ζ (dot-dashed) results. On the left-hand side, $\mu = m$ while on the right-hand side, $\mu = 2m$

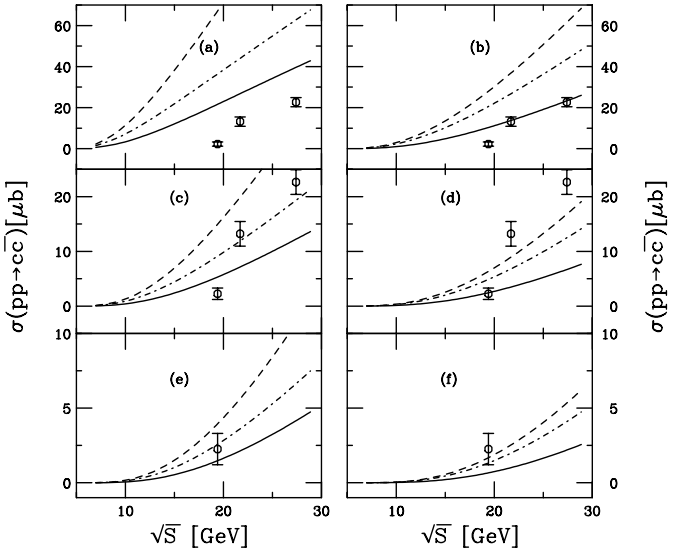

Fig. 17. The energy dependence of $c\bar{c}$ production in pp collisions with, **a** and **b**, $m = 1.2$, **c** and **d**, $m = 1.5$, and, **e** and **f**, $m = 1.8\,\mathrm{GeV}$, calculated with the MRST2002 NNLO proton densities. We show the NLO (solid), 1PI NNLO-NNLL (dashed) and 1PI NNLO-NNNLL+ζ (dot-dashed) results. On the left-hand side, $\mu = m$ while on the right-hand side, $\mu = 2m$

with the two highest energy data points than the exact NLO. The 1PI NNLO cross sections are in rather good agreement with the data when $m = \mu = 1.5\,\mathrm{GeV}$ is used with the MRST2002 NNLO parton densities. Indeed, the 1PI NNLO-NNNLL+ζ result in Fig. 17c agrees rather well with the two higher energy data points. Thus, as in [4], we can conclude that the full NNLO result can likely describe the charm data well with $m = \mu = 1.5\,\mathrm{GeV}$ whereas the lower mass is needed with an NLO calculation alone.

Table 1 gives the charm cross sections in pp collisions at two energies, $\sqrt{S} = 6.98\,\mathrm{GeV}$, the future GSI energy, and 17.3 GeV, the CERN SPS ion energy. We present results for both the MRST2002 NNLO and GRV98 parton densities based on a central value of $m = \mu = 1.5\,\mathrm{GeV}$. (The choice of mass and scale used for our central value is for better illustration of the uncertainties rather than any fit to data.) The first uncertainty is due the scale choice. Since we do not calculate the result for $\mu = m/2$ here, we show only the difference between the values of $\mu = m$ and $2m$. The second uncertainty is that due to the charm quark mass. The exact NLO and the 1PI NNLO-NNNLL+ζ cross sections are shown. Note that the differences between the MRST2002 and GRV98 densities are larger for charm since the difference in the values of Λ_3 between the two sets is larger than that for Λ_4. The relative increase of the NNLO-NNNLL+ζ cross section is highest at the lower energy with an increase over the NLO result by a factor of 2.6 for the MRST densities and 2.2 for the GRV98. At 17.3 GeV, the increase is by a factor of 1.8 and 1.5 respectively. Thus the importance of the near-threshold corrections is reduced further from the charm production threshold, as might be expected.

In Figs. 18 and 19, we compare the pp K factors for GRV98 HO and MRST2002 NNLO respectively. The same

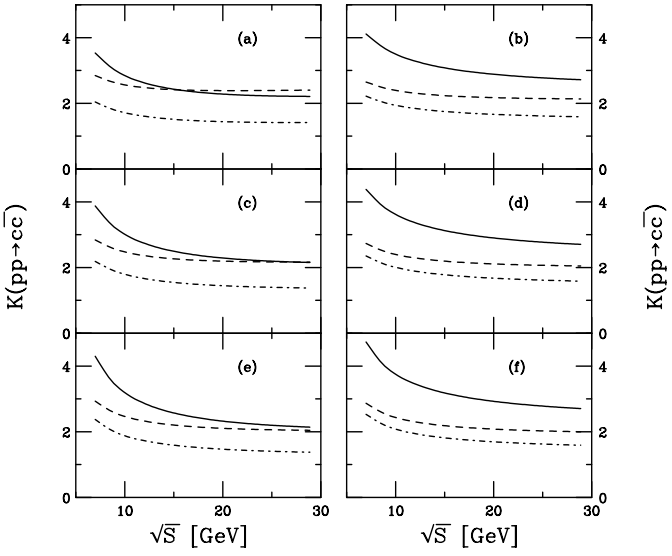

Fig. 18. The K factors for $c\bar{c}$ production in pp collisions with, **a** and **b**, $m = 1.2$, **c** and **d**, $m = 1.5$, and, **e** and **f**, $m = 1.8\,\mathrm{GeV}$, calculated with the GRV98 HO parton densities. We present $K_0^{(1)}$ (solid), $K^{(2)}$ (dashed) and $K_{\mathrm{sub}}^{(2)}$ (dot-dashed) for $\mu = m$ (left-hand side) and $\mu = 2m$ (right-hand side)

Table 1. The $c\bar{c}$ production cross sections in pp collisions at $\sqrt{S} = 6.98$ and 17.3 GeV. The exact NLO results and the approximate NNLO-NNNLL+ζ results, based on $m = \mu = 1.5\,\mathrm{GeV}$, are shown. The first uncertainty is due to the scale choice, the second, the charm quark mass

		σ (μb)	
$\sqrt{S}$ (GeV)	Order	MRST2002 NNLO	GRV98
6.98	NLO	$0.034 - 0.027\,^{+\,0.56}_{-\,0.032}$	$0.028 - 0.022\,^{+\,0.42}_{-\,0.026}$
6.98	NNLO-NNNLL+ζ	$0.09 - 0.07\,^{+\,1.4}_{-\,0.085}$	$0.061 - 0.05\,^{+\,0.9}_{-\,0.057}$
17.3	NLO	$3.8 - 2.1\,^{+\,13}_{-\,2.8}$	$2.8 - 1.4\,^{+\,8.3}_{-\,2}$
17.3	NNLO-NNNLL+ζ	$6.7 - 3.4\,^{+\,22.5}_{-\,4.9}$	$4.1 - 1.8\,^{+\,12.2}_{-\,3}$

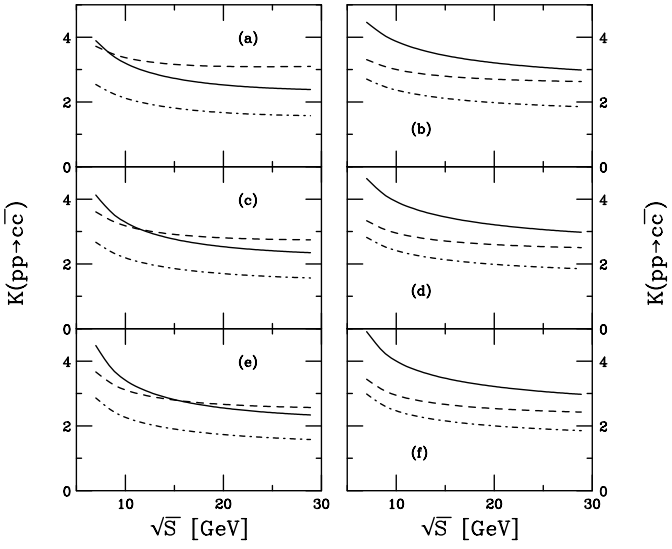

Fig. 19. The K factors for $c\bar{c}$ production in pp collisions with, **a** and **b**, $m = 1.2$, **c** and **d**, $m = 1.5$, and, **e** and **f**, $m = 1.8\,\mathrm{GeV}$, calculated with the MRST2002 NNLO parton densities. We present $K_0^{(1)}$ (solid), $K^{(2)}$ (dashed) and $K_{\mathrm{sub}}^{(2)}$ (dot-dashed) for $\mu = m$ (left-hand side) and $\mu = 2m$ (right-hand side)

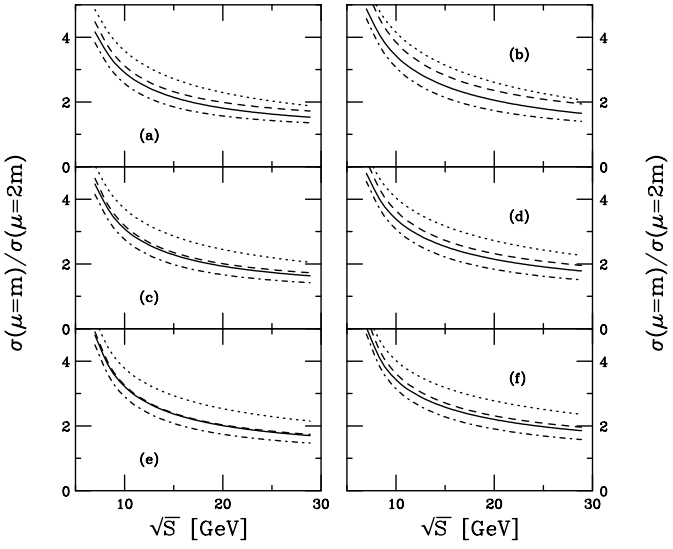

Fig. 20. The scale dependence of $c\bar{c}$ production in pp collisions with, **a** and **b**, $m = 1.2$, **c** and **d**, $m = 1.5$, and, **e** and **f**, $m = 1.8\,\mathrm{GeV}$. We give the ratios $\sigma(\mu = m)/\sigma(\mu = 2m)$ for the LO (dotted), NLO (solid), 1PI NNLO-NNLL (dashed) and 1PI NNLO-NNNLL+ζ (dot-dashed) cross sections. Results with the GRV98 HO densities are given on the left-hand side while the MRST2002 NNLO results are shown on the right-hand side

trends are seen as in $\pi^- p$ interactions although the energy dependence at low $\sqrt{S}$, particularly for $K^{(1)}$, is stronger. None of the K factors are strong functions of mass, scale or parton density. The parton density dependence is thus reduced relative to the calculations with CTEQ5M shown in [4]. This is perhaps because the CTEQ5M gluon density is higher than either the GRV98 HO or MRST2002 NNLO gluon densities at $x \leq 0.1$ and at the low charm production scales. Although the initial scales of the CTEQ5 and MRST sets are not very different, $1\,\mathrm{GeV}^2$ for CTEQ5M and $1.25\,\mathrm{GeV}^2$ for MRST2002, the low x behavior is quite different. Indeed at low scales, when $m = \mu = 1.2\,\mathrm{GeV}$, the CTEQ5M gluon distribution is essentially constant as $x \to 0$ with the tail of the distribution appearing at $x \approx 0.1$, while for the MRST2002 NNLO set the gluon distribution becomes negative at $x < 0.001$ and peaks at $x < 0.1$. When μ is increased to $2m$ for the same mass, the CTEQ5M density decreases with increasing x while the MRST2002 NNLO density peaks around $x \approx 0.001$, decreasing at lower x. Although our calculations are not sensitive to the very low x region, the different low-x behavior affects the gluon distributions at higher x. The lower MRST gluon density, combined with the lower Λ_3 relative to CTEQ5M reduces the higher-order corrections and hence the K factors. Thus $K_{\mathrm{sub}}^{(2)}$ varies between 1.3 and 1.7 for GRV98 HO and 1.5 to 1.9 for MRST2002 NNLO when $\sqrt{S} \geq 15\,\mathrm{GeV}$, significant improvements over the 1PI NNLO-NNLL results, $K^{(2)} \approx 2$–2.4 for GRV98 HO and 2.5–3 for MRST2002 NNLO and CTEQ5M. In addition, $K_{\mathrm{sub}}^{(2)} < K_0^{(1)}$ for all cases considered, not a feature of the 1PI NNLO-NNLL result.

We compare the scale dependence of the cross sections in Fig. 20. The GRV98 HO cross section ratios on the left-hand side are compared to the MRST2002 NNLO ratios on the right-hand side. The scale dependence is similar

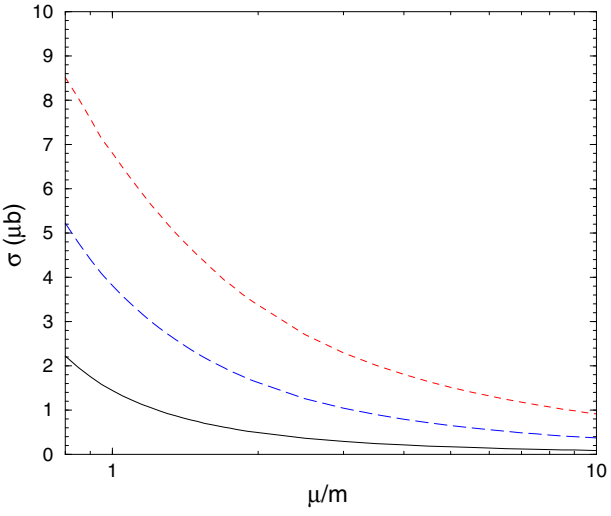

Fig. 21. The charm production cross section as a function of μ/m at $\sqrt{S} = 17.3\,\mathrm{GeV}$ with $m = 1.5\,\mathrm{GeV}$ and the MRST2002 NNLO parton densities. We show the Born (solid), NLO (long-dashed) and NNLO-NNNLL+ζ (dashed) results

for the two sets of parton densities although the MRST scale dependence is somewhat stronger at low $\sqrt{S}$. The 1PI NNLO-NNNLL+ζ scale dependence is reduced relative to the 1PI NNLO-NNLL dependence which is stronger than the exact NLO dependence for most values of mass. Indeed the 1PI NNLO-NNLL ratios are only similar to the NLO ratios for $m = 1.8\,\mathrm{GeV}$ while the 1PI NNLO-NNNLL+ζ ratios are lower than the rest of the calculated ratios for all masses.

In Fig. 21 we plot the scale dependence for $0.8 < \mu/m < 10$ at $\sqrt{S} = 17.3\,\mathrm{GeV}$ and $m = 1.5\,\mathrm{GeV}$. We show results for

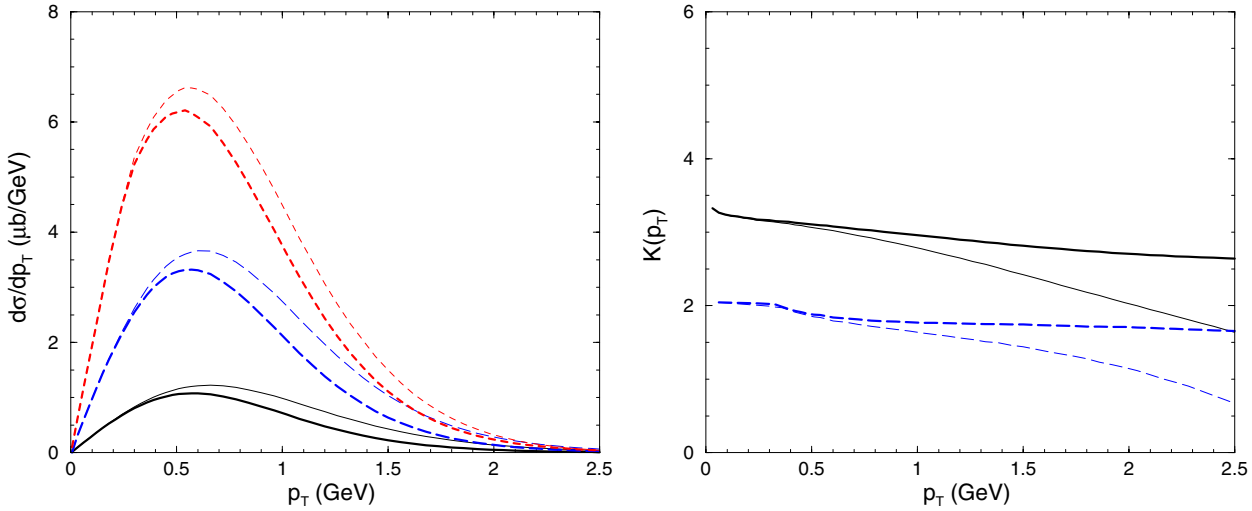

Fig. 22. The charm quark transverse momentum distributions at $\sqrt{S} = 17.3\,\text{GeV}$ and $m = 1.5\,\text{GeV}$ with the MRST2002 NNLO parton densities. On the left-hand side we show the Born (solid), NLO (long-dashed), and NNLO-NNNLL+ζ (dashed) results while on the right-hand side we present $K_0^{(1)}$ (solid) and $K_{\text{sub}}^{(2)}$ (dashed). The bold lines are calculated with $\mu = m_{\text{T}}$ while the thin lines are with $\mu = m$

the Born, NLO, and NNLO-NNNLL+ζ cross sections. None of the cross sections show a plateau at any value of μ/m, as seen for the NLO and NNLO $b\bar{b}$ cross sections in Fig. 11. However, the relative dependence of the cross section on μ/m decreases as the accuracy of the cross section increases.

Figure 22 shows the charm quark transverse momentum distributions in pp collisions at $\sqrt{S} = 17.3\,\text{GeV}$, $m = 1.5\,\text{GeV}$, and two scales, $\mu = m$ and $\mu = m_{\text{T}} = \sqrt{p_{\text{T}}^2 + m^2}$. The Born, NLO, and NNLO-NNNLL+ζ results are shown on the left-hand side. On the right-hand side we plot $K_0^{(1)}$ and $K_{\text{sub}}^{(2)}$. Again the enhancement in the p_{T} distribution is similar to that seen for the total cross sections in Fig. 19. The behavior of the K factors as a function of p_{T} is similar to that in Fig. 12.

5 Conclusions

In this paper we have calculated soft NNLO corrections to the bottom and charm quark total cross sections and transverse momentum distributions in hadron–hadron collisions. We have added new subleading soft NNNLL terms and some virtual terms, including all soft-plus-virtual factorization and renormalization scale-dependent terms. We have found that these new subleading corrections reduce the size of the NNLO cross sections, and thus the K factors, as well as diminish the scale dependence of the cross section.

Acknowledgements. The research of N.K. has been supported by a Marie Curie Fellowship of the European Community programme "Improving Human Research Potential" under contract number HPMF-CT-2001-01221. The research of R.V. is supported in part by the Division of Nuclear Physics of the Office of High Energy and Nuclear Physics of the U.S. Department of Energy under Contract No. DE-AC-03-76SF00098.

References

1. N. Kidonakis, Phys. Rev. D **64**, 014009 (2001)
2. N. Kidonakis, E. Laenen, S. Moch, R. Vogt, Phys. Rev. D **64**, 114001 (2001)
3. N. Kidonakis, E. Laenen, S. Moch, R. Vogt, Nucl. Phys. A **715**, 549c (2003)
4. N. Kidonakis, E. Laenen, S. Moch, R. Vogt, Phys. Rev. D **67**, 074037 (2003)
5. N. Kidonakis, R. Vogt, Phys. Rev. D **68**, 114014 (2003); in EPS-HEP 2003, hep-ph/0309045
6. N. Kidonakis, G. Sterman, Phys. Lett. B **387**, 867 (1996); Nucl. Phys. B **505**, 321 (1997)
7. N. Kidonakis, G. Oderda, G. Sterman, Nucl. Phys. B **525**, 299 (1998); B **531**, 365 (1998); N. Kidonakis, Int. J. Mod. Phys. A **15**, 1245 (2000)
8. E. Laenen, G. Oderda, G. Sterman, Phys. Lett. B **438**, 173 (1998)
9. For plans for the future facility, see the GSI home page, http://www.gsi.de
10. N. Kidonakis, Int. J. Mod. Phys. A **19**, 1793 (2004)
11. A.D. Martin, R.G. Roberts, W.J. Stirling, R.S. Thorne, Eur. Phys. J. C **28**, 455 (2003)
12. P. Bordalo et al. (NA10 Collaboration), Z. Phys. C **39**, 7 (1988)
13. M.G. Catanesi et al. (WA78 Collaboration), Phys. Lett. B **231**, 328 (1989)
14. M. Adamovich et al. (Beatrice Collaboration), Nucl. Phys. B **519**, 19 (1998)
15. K. Kodama et al. (E653 Collaboration), Phys. Lett. B **303**, 359 (1993)
16. R. Jesik et al. (E672-E706 Collaborations), Phys. Rev. Lett. **74**, 495 (1995)
17. M. Glück, E. Reya, A. Vogt, Eur. Phys. J. C **5**, 461 (1998)
18. M. Glück, E. Reya, I. Schienbein, Eur. Phys. J. C **10**, 313 (1999)
19. J. Smith, R. Vogt, Z. Phys. C **75**, 271 (1997)
20. R. Vogt, Heavy Ion Phys. **17**, 75 (2003) [hep-ph/0207359]
21. H.L. Lai et al., Eur. Phys. J. C **12**, 375 (2000)

22. D.M. Jansen et al. (E789 Collaboration), Phys. Rev. Lett. **74**, 3118 (1995)
23. T. Alexopoulos et al. (E771 Collaboration), Phys. Rev. Lett. **82**, 41 (1999)
24. I. Abt et al. (HERA-B Collaboration), Eur. Phys. J. C **26**, 345 (2003)
25. N. Kidonakis, J. Smith, Phys. Rev. D **51**, 6092 (1995); hep-ph/9506253
26. R. Vogt, Z. Phys. C **71**, 475 (1996)
27. S. Frixione, M.L. Mangano, P. Nason, G. Ridolfi, Nucl. Phys. B **431**, 453 (1994)
28. S. Frixione, M.L. Mangano, P. Nason, G. Ridolfi, Adv. Ser. Direct High Energy Phys. **15**, 609 (1998)
29. S. Barlag et al. (ACCMOR Collaboration), Z. Phys. C **39**, 451 (1988)
30. G.A. Alves et al. (E769 Collaboration), Phys. Rev. Lett. **77**, 2388 (1996)
31. S. Barlag et al. (ACCMOR Collaboration), Z. Phys. C **49**, 555 (1991)
32. M.I. Adamovich et al. (WA92 Collaboration), Nucl. Phys. B **495**, 3 (1997)
33. M. Aguilar-Benitez et al. (LEBC-EHS Collaboration), Phys. Lett. B **161**, 400 (1985)
34. M. Aguilar-Benitez et al. (LEBC-EHS Collaboration), Z. Phys. C **40**, 321 (1988)
35. G.A. Alves et al. (E769 Collaboration), Phys. Rev. Lett. **70**, 722 (1993)
36. M.J. Leitch et al. (E789 Collaboration), Phys. Rev. Lett. **72**, 2542 (1994)
37. R. Vogt, Int. J. Mod. Phys. E **12**, 211 (2003) [hep-ph/0111271]